SAND2010-0252C

Demonstration of Thermal Emissions Control

A. A. Cruz-Cabrera[a], S. A. Kemme[a], M. J. Cich[a], A. R. Ellis[a], J. R. Wendt[a], A. M. Rowen[a], S. Samora[b], M. J. Martinez[a], D. A. Scrymgeour[a], D. W. Peters[a]

[a]Sandia National Laboratories, Albuquerque, NM 87185-1082
[b]LMATA, Albuquerque, NM, 87109, USA

ABSTRACT

In this paper we describe our efforts to control the thermal emission from a surface utilizing structured surfaces with metal/dielectric interfaces. The goal was not to eliminate emissions, but to control the output direction and spectrum. We describe the fabrication and measurement of large passive devices (15x15 mm) and arrays of smaller chips for thermal emission control in the longwave infrared (8 to 12 μm) spectral region. All the devices consist of a metal base layer covered with dielectric/metal posts or lines, 0.5 microns tall. The posts (0.9x0.9 μm) and lines (0.3 μm wide) are sub-wavelength. One-dimensional and two-dimensional devices with a 3 micron pitch will be shown. The devices are measured with both a hemispherical directional reflectometer and a variable angle directional emissometer. Both simulated and experimental results show the thermal emissions effectively limited to a small spectral region and grazing angles from the surface (≥ 80º) in stark contrast to the typical Lambertian radiation seen from unstructured material. Finally, the effect of this thermal emission control is illustrated using an infrared camera.

Keywords: Emission, absorption, plasmons, diffractive, gratings, infrared, thermal, planarization, release.

1. INTRODUCTION

The surface of any material radiates energy that is usually incoherent and quasi-isotropic. The radiation is a function of the temperature of the material and the typical radiation patterns are Lambertian and broadband, as in Figure 1(a), mostly in the infrared (IR). These thermal emissions are treated as noise sources that are difficult to manage, and even more difficult to reduce. There is a considerable body of work in the field of control of thermal emission. Research has focused on the use of polar materials (e.g. silicon carbide) and verifying the coherence of device emission,[2] photonic crystals in Ge at near infrared wavelengths,[3] thermo photovoltaic applications using simple and complex gratings[4-5] and photonic crystals in tungsten.[6-7] Work has also been done with one-dimensional photonic crystals in silicon nitride and silicon dioxide or multi-stack thin films,[8] and gratings in lithium fluoride and germanium for LWIR wavelengths.[9] Our work differentiates from previously described research in that we focus on converting Lambertian thermal emission to antenna patterns that emit at glancing angles using simple one- and two-dimensional structures. We also look at the overall spectral response of the devices from 2 to 13 μm (MWIR and LWIR). Most of the previous work reported results in 2 or 3 narrow wavelength ranges which do not give a complete picture of the device response. Many of the previously reported devices have narrow wavelength band and angle responses.

If the incoherent thermal emission could be made coherent, the IR emission could be modified into desirable radiation lobes that resemble an antenna pattern [Figure 1(b)]. We have fabricated and tested parts that structure the surface of the material on the same scale as the emitted wavelength at a metal/dielectric interface that enables us to propagate a near field into the far field by using coherent effects. This structuring was done in the lateral and depth direction. The lateral structuring consisted of gratings on top of a metal surface and the depth structuring was done by stacking films. The next section quickly reviews Kirchoff's Law and its importance in determining the proper method for measuring these devices. Sections 3 and 4 describe silicon nitride and silicon dioxide based devices and their measurement. Section 5 briefly presents the feasibility of using smaller device sizes and Section 6 demonstrates the effect of the tailored emission profiles using an infrared camera.

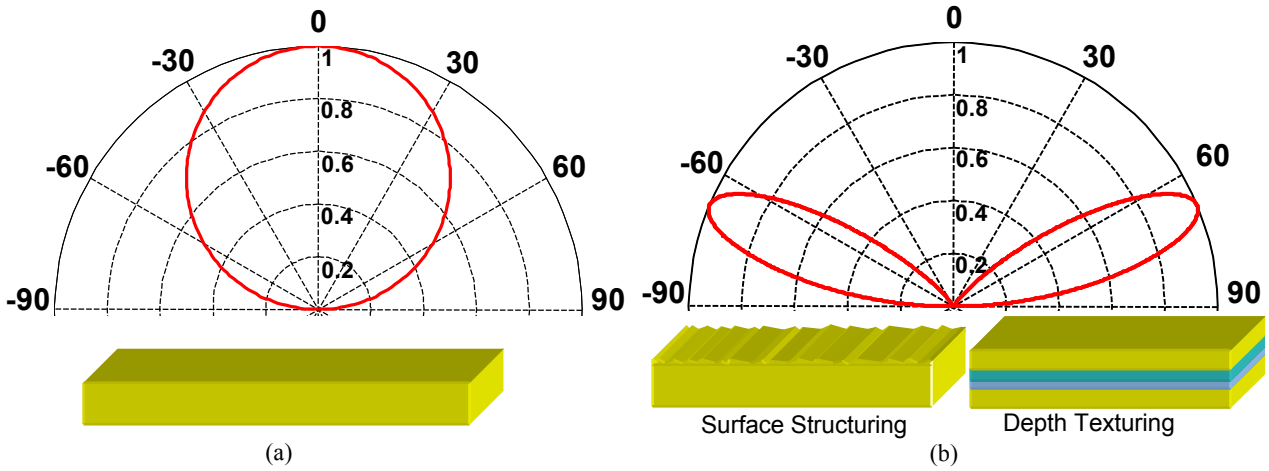

(a) (b)

Figure 1. Panel (a) shows a typical Lambertian angular emission. Panel (b) shows a directed thermal emission due to surface structuring or depth texturing.

2. USING THE GENERAL FORM OF KIRCHHOFF'S LAW

We start with the main assumption that a gray body will have absorption, α, reflection, Rx, and transmission, Tx; and their sum will total one:

$$1 = \alpha(\lambda, \beta, \theta, T) + Rx(\lambda, \beta, \theta, T) + Tx(\lambda, \beta, \theta, T) \tag{1}$$

Where λ is the spectral dependence, β and θ are the azimuthal and circumferential angles, and T is the temperature of the gray body. By setting the body to not have a significant transmission (e.g. covering the body's surfaces with a metal that is thick enough not to transmit at the spectral region of interest), Equation (1) can be reduced to:

$$\alpha(\lambda, \beta, \theta, T) = 1 - Rx(\lambda, \beta, \theta, T) \tag{2}$$

The absorption is now a function of the reflection. The general form of Kirchhoff's law defines that at thermal equilibrium directional emissivity, ε, is equal to the directional absorptivity[1]:

$$\varepsilon(\lambda, \beta, \theta, T) = \alpha(\lambda, \beta, \theta, T) \tag{3}$$

By modifying equation (3) with equation (2), we get an equation form that looks at directional emissivity as a function of reflectivity, a parameter that we can easily measure:

$$\varepsilon(\lambda, \beta, \theta, T) = 1 - Rx(\lambda, \beta, \theta, T) \tag{4}$$

As will be shown, both reflectivity measurements and direct emissivity measurements give similar results. This verifies the use of reflectivity measurements when the underlying metal layer is thick enough to effectively suppress any transmitted signal.

3. SILICON NITRIDE DESIGN

A significant effort was made to determine the best candidate materials for these devices. The results of this effort were designs utilizing a silicon nitride grating with a gold layer underneath and gold caps on the grating lines, see Figure 2. Specifically, the device consists of a metal film with high reflectivity (>97%) and is optically thick at the working

wavelengths, as in Figure 2(a). A less reflective metal will show emissions/absorptions at normal angles. We selected gold and aluminum, both with reflectivity larger than 98% in our waveband of interest. The line grating is 0.3μm (10% fill factor) of non-stoichiometric silicon nitride with a 0.2μm thick gold cap. Parts were fabricated on gallium arsenide, Figure 2(b), and silicon substrates. The only requirement for the substrate is that it is rigid and compatible with the device fabrication process.

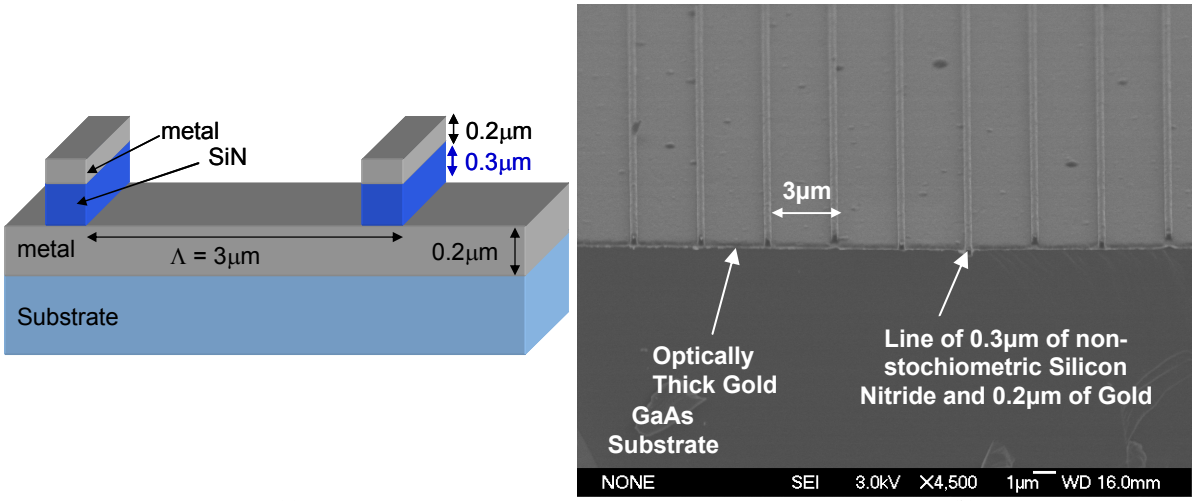

(a) (b)

Figure 2. Panel (a) shows a grazing-emission component design consisting of a 200nm planar layer of metal topped with a grating consisting of a 300 nm non-stoichiometric silicon nitride and a 200 nm layer of metal. Panel (b) shows a SEM micrograph of a cross section of a 3μm period line grating on top of optically thick gold (0.2μm).

The parts were fabricated by depositing 0.2μm of gold and 0.3μm of Si_3N_4 on a silicon or gallium arsenide substrate, Figure 3. Polymethyl methacrylate (PMMA) was spun on top of the substrate and patterned with an e-beam writer. For the two-dimensional patterned parts the features are big enough so that photoresist and a stepper can replace the PMMA and the e-beam writer. 0.2μm of gold is evaporated on top of the developed PMMA, followed by liftoff of the PMMA. The patterned gold is used as a mask to etch the silicon nitride. The silicon nitride deposited is not perfectly stoichiometric due to the lower temperatures and incorporated hydrogen of the deposition process employed.

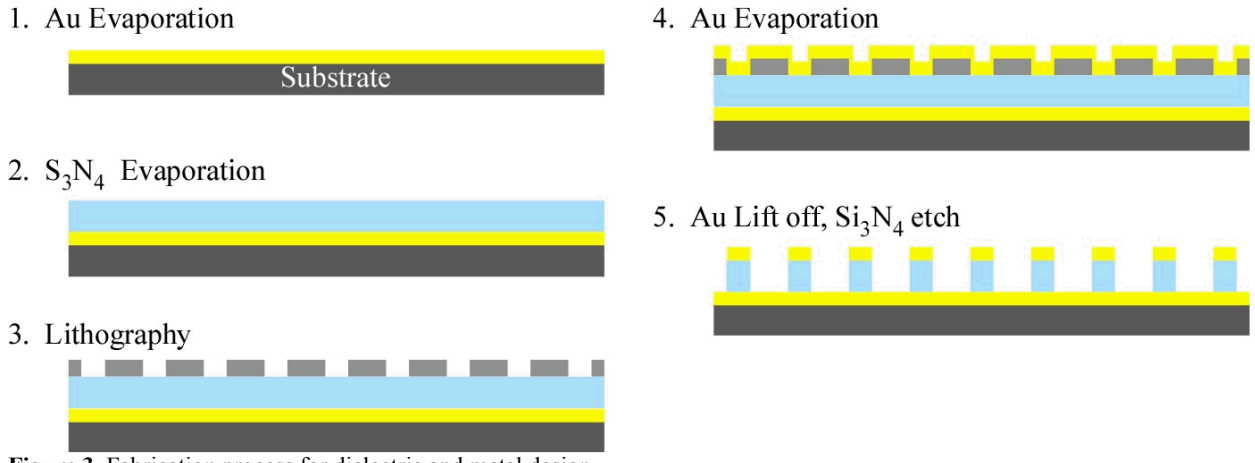

Figure 3. Fabrication process for dielectric and metal design.

Figure 4(a) shows the RCWA simulation of the absorption/emission performance of the device in Figure 2(a). The graph indicates a high, almost isolated absorption/emission centered at 10.1μm, with a width of ±1μm, and a peak at an angle of 85 degrees. We believe that this absorption/emission occurs due to the strong silicon nitride absorption band around 10μm and its interface with gold film, the periodic gold caps, and its interface with air. The graph barely shows

the surface plasmon due to the 3µm grating in gold that interfaces with air. Figure 4(b) shows the hemispherical directional reflectometer (HDR) measurement of a part made using gold for the metal film and line metal caps. The graph shows the absorption centered at a wavelength of 10.4µm. Given that the HDR cannot reliably measure beyond 75 degrees, we are not able to see the peak signal in this measurement. Notice the surface plasmon for the 3µm grating and the corresponding artifact from the pickup optics of the HDR. Figure 4(c) is the actual thermal emission measurement using a variable angle directional emissometer (VADE).[12] The wavelength center of the emission of interest is at 10.4µm and the emission graph barely shows the surface plasmon for the 3µm grating. The emission measurement is limited in angle from 0 to 80 degrees. (Stoichiometric Si_3N_4 changes the performance only slightly. The absorption/emission from a stoichiometric component is centered close to 9.7µm, the exact position depends on the hydrogen content.)

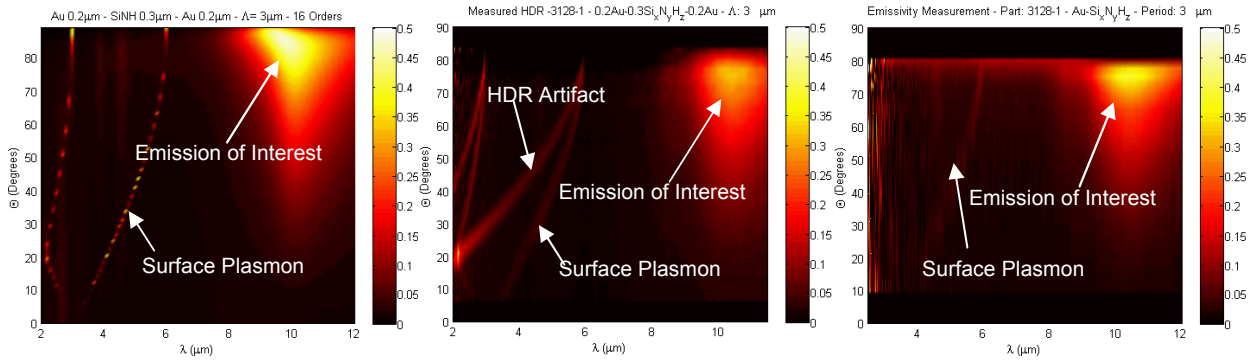

(a) (b) (c)

Figure 4. Panel (a) RCWA simulation of absorption for silicon nitride grating (with 0.2µm gold cap) on top of gold film introduced in Figure 2. Panel (b) shows the measured absorption using an HDR and obtaining similar results. Panel (c) shows the actual emission measurement of the same part in panel (b) with identical results.

To eliminate the need to rotationally align the devices we created a part with two-dimensional features. The device has square posts, shown in Figure 5, with the same 3µm periodicity in both axes. The part has the same metal and silicon nitride thickness as the one-dimensional grating part described above. The posts are 0.9µm on the side, to maintain the same 10% fill factor, of non-stoichiometric silicon nitride with a 0.2µm thick gold cap on top. The optically thick gold is at least 0.2µm thick.

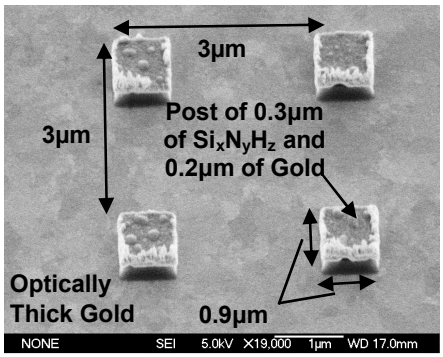

Figure 5. SEM micrograph of a 3µm period, two-dimensional array of posts on top of optically thick gold film.

Figure 6(a) shows the absorption/emission RCWA simulation for the designs with two-dimensional posts. The simulation shows the same absorption/emission around 85 degrees and centered at a wavelength of 10µm. The main difference is a strong absorption/emission around 3.5µm, between normal and 10 degrees. Figure 6(b) shows the measurement using the HDR. The measurement shows similar results as Figure 4(b) with the exception of the HDR measurement artifact, and the signal near normal incidence at ~3.5µm, which we are still trying to determine its nature. Finally, Figure 6(c) shows the direct measurement of the emission of this part using the VADE. All panels show a very

similar response to the one-dimensional part with the exception of the low angle emission at ~3.5 µm. Figure 7(a) shows the polar response at a wavelength of 10.21µm (peak emission) from the VADE measurement.

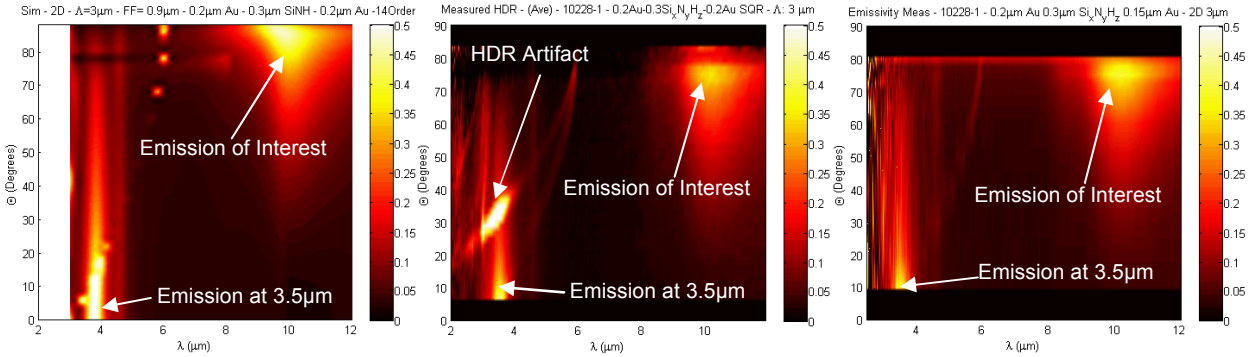

(a) (b) (c)

Figure 6. Panel (a) RCWA simulation of absorption for two-dimensional silicon nitride grating introduced in Figure 5. Panel (b) shows the measured absorption of the same design using an HDR and obtaining close to the same results of the RCWA. Panel (c) shows the emission measurement of the part with similar results to the ones shown in Figure 4(c).

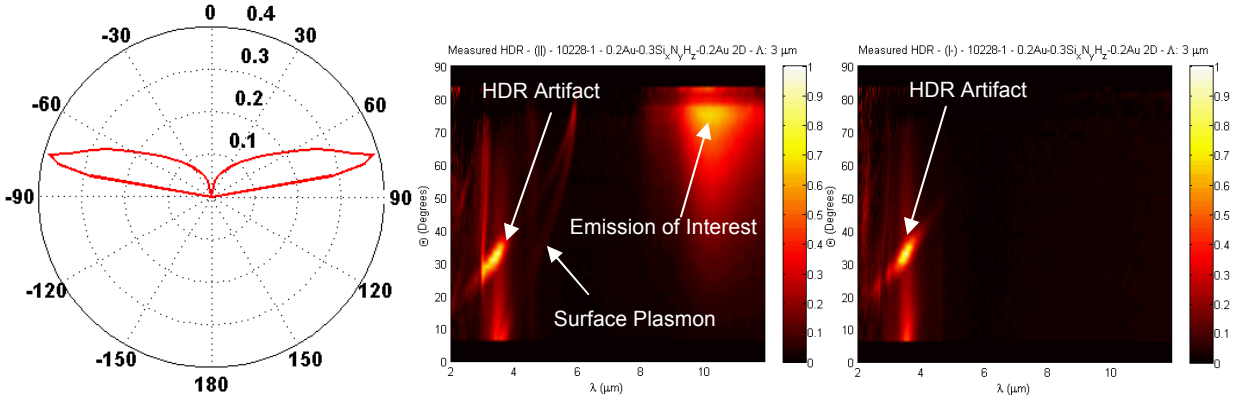

(a) (b) (c)

Figure 7. Panel (a) shows the polar response of the part at the wavelength of 10.21µm. Panel (b) shows the measured absorption of two-dimensional array of posts for the s-polarization. Panel (c) shows the absorption measurement for the p-polarization.

The same two-dimensional part was tested with the HDR to measure the polarization states of the absorption/emission. Figure 7(b) shows that the emission of interest at 10µm and 85 degrees is of the p-polarization state, similar to the barely noticeable surface plasmon centered at 3µm. Figure 7(c) shows the lack of absorption/emission for the s-polarization at a wavelength of 10µm. The only emission seen also exists in the p-polarization analysis and is related to the HDR artifact from the obscuration of the pickup optics and the emission between normal and 10 degrees at 3.5µm, seen at both polarizations. Notice that the HDR artifact does not show in the actual emissivity measurement in Figure 6(c).

4. SILICON DIOXIDE DEVICE

Parts were fabricated with silicon dioxide replacing the silicon nitride and using the same geometrical dimensions as the devices presented in Figure 2(a). An RCWA simulation of the part is shown in Figure 8(a) where the most salient feature of the simulation is the shift in wavelength of the absorption/emission towards 9µm and the narrow absorption/emission down to 20 degrees. Figure 8(b) shows the measurement using the HDR of a part made with 0.3µm of silicon dioxide. The part has 0.2µm gold cap. The measurement shows similar data as the simulation up to 79 degrees; though, the data is only reliable to 75 degrees.

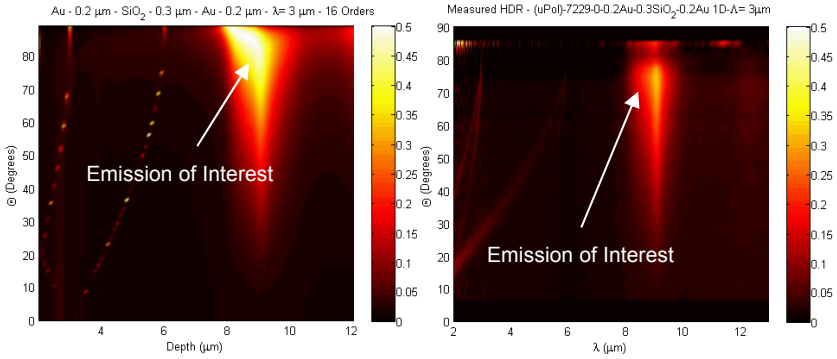

(a) (b)

Figure 8. (a) RCWA simulation of absorption for silicon dioxide grating on top of gold film. The graph shows high absorptions at angles close to 80 degrees at a wavelength of 9µm. Panel (b) shows the measured absorption of similar part using an HDR.

5. ARRAY OF SMALLER PARTS

Parts were fabricated using aluminum, instead of gold for the bottom and top layers. We obtained the same results [Figure 9(a)] as with the part made of gold (see Figure 4). The part fabricated with aluminum was scribed and broken into fifteen parts, each 3 by 3 millimeters and tested as an array [see Figure 9(b)]. The performance was similar to the performance of the original part.

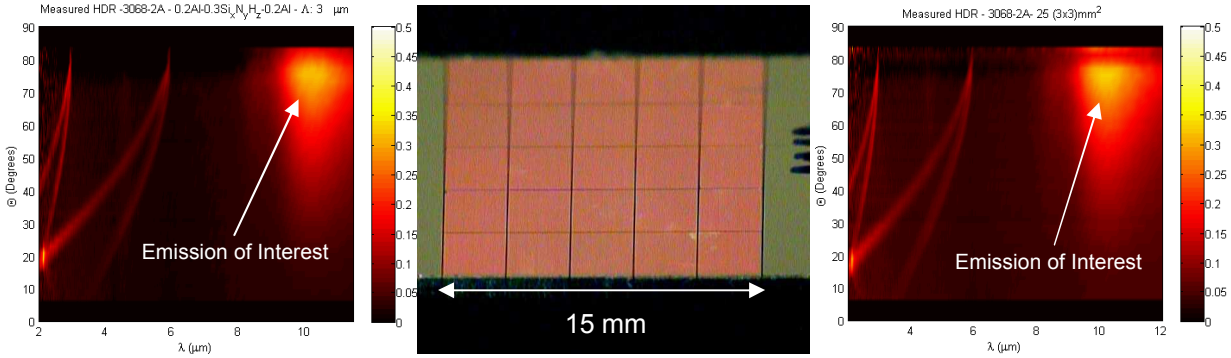

(a) (b) (c)

Figure 9. Panel (a) shows absorption from HDR measurement for silicon nitride grating (with a 0.2µm aluminum cap) on top of 0.2µm aluminum film, with similar geometry to the one introduced in Figure 2. Panel (b) shows the same part after scribe and break. Panel (c) shows absorption from HDR measurement from the part after scribe and break.

6. INTEGRATED CAMERA MEASUREMENT

Infrared pictures were taken of selected bulk parts with a FLIR ThermaCAM S60 infrared camera. The imaging pixels are microbolometers, which measure IR radiation through changes in detector material electrical resistivity due to impinging IR radiation. It has a spectral band response from 7 to 13 µm, and a noise equivalent temperature difference (NEDT) of 60-70 mK.

The microbolometer camera measures an integrated response over its entire spectral window. As such, it does not see "colors" but rather intensity. Therefore, the camera images should be interpreted as intensity maps of IR light striking the camera at any wavelength. For example, a bright object in an IR image could be emitting across the complete spectral window or at a very specific wavelength, but there is no way to distinguish between the two. This intensity gradient is shown as a false color image that goes from as the intensity of the IR radiation increases.

Two parts were placed on a gold-coated surface along with a piece of glass. The substrate was placed on a heater that was set to 60°C. The thermal imager measured the glass piece as approximately 40°C, which was probably close in temperature to the devices. At normal incidence (left panel of Figure 10), notice the glass appears very bright, compared to both devices. We can start to see both parts beginning to glow as the angle of view is increased. Both parts fabricated with Si_3N_4 and SiO_2 look approximately the same in the IR image, despite each having slightly different wavelength response (compare Figure 4 to Figure 8). This is because the camera measures intensity only, and not wavelength, as discussed above.

Figure 10 clearly demonstrates two important points. One is that normal materials at any temperature (the glass in Figure 10) have bright thermal emission at any angle due to their Lambertian emission (see Figure 1). The second is that the devices have been specifically designed to emit only at high angles, and therefore, only look bright when viewed from grazing angles.

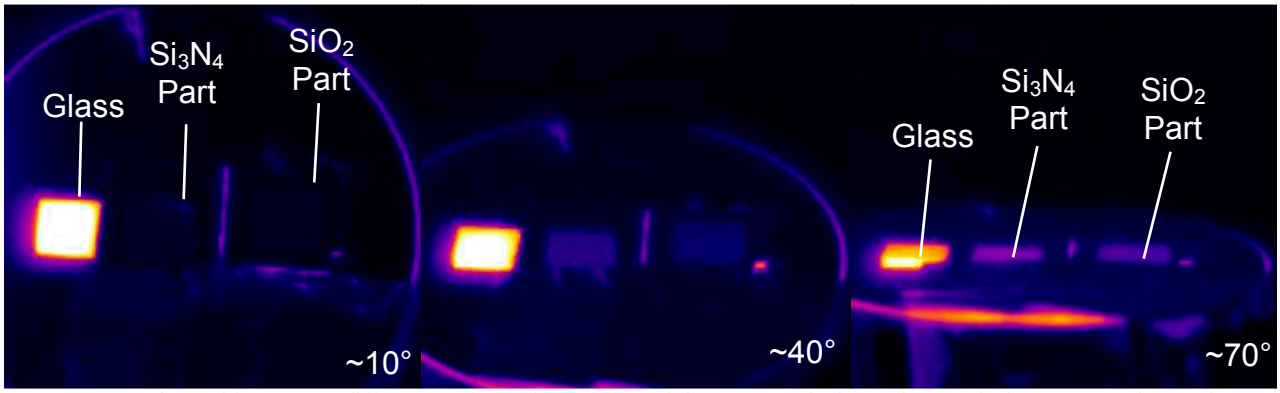

Figure 10. IR thermal images, at different angles of inclination, of the parts made from Si_3N_4 and SiO_2 compared to a piece of glass. The glow on the bottom of the right panel is the edge of the silicon substrate emitting in the same fashion as the glass.

Similar measurement with the camera was taken with the array of 25 chips (3 by 3 millimeter in aluminum) and was compared to the large 15 by 15 millimeter part and a piece of glass, see Figure 11. The camera indicates similar results between the array and the large part.

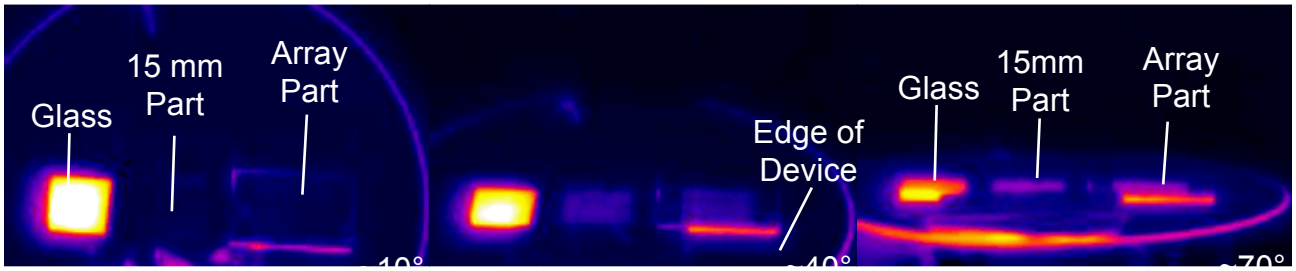

Figure 11. IR thermal images at different angles of inclination of the large 15mm part and the 5 by 5 array of chips, all compared to a piece of glass. The glow on the bottom of the right panel is the edge of the silicon substrate emitting in the same fashion as the glass.

8. CONCLUSIONS

This project has allowed us to successfully design, fabricate, and measure structured devices at the lateral and depth dimensions that modify the characteristic Lambertian and wide spectral emission from the surface of a gray body. These devices change the thermal emission to 1μm narrow bands centered at wavelengths of 9 and 10 microns, and the peak emission were restricted to grazing angles around 85 degrees from normal and the absorptions/emissions are s-polarized.

Devices were fabricated in gold or aluminum for the base film and a cap of the same metal on top of the dielectric. We expect that a part fabricated using a good metal, like silver, will have similar performance. Parts were fabricated using a non-stoichiometric silicon nitride with emissions centered at 10 microns. Using a stoichiometric nitride film slightly shifts the film performance to the blue. Other parts were fabricated using silicon dioxide with emissions centered at 9 microns.

A part made in Aluminum was scribed and broken into 25 pieces and was tested as an array with similar performance as the original piece. Arrays of smaller pieces can be used to control thermal emissions on non-planar surfaces.

ACKNOWLEDGMENTS

Sandia is a multiprogram laboratory operated by Sandia Corporation, a Lockheed Martin Company, for the United States Department of Energy's National Nuclear Security Administration under contract DE-AC04-94AL85000.

REFERENCES

1. R. Seigel and J.R. Howell, *The Blackbody, Electromagnetic Theory, and Material Properties*. Thermal Radiation Heat Transfer. Vol. 1. 1968, Washington D.C.: NASA.
2. J.J. Greffet, R. Carminati, K. Joulain, J.P. Mulet, S.P. Mainguy and Y. Chen, Nature, 416, 61 (2002).
3. M. Laroche, R. Carminati and J.J. Greffet, Phys Rev Lett, 96, 123903 (2006).
4. C.J. Fu, Z.M. Zhang and D.B. Tanner, Opt Lett, 30, 1873 (2005).
5. A. Heinzel, V. Boerner, A. Gombert, B. Blasi, V. Wittwer and J. Luther, Journal of Modern Optics, 47, 2399 (2000).
6. A. Gombert, AIP Conference Proceedings, 123 (2003).
7. M.U. Pralle, M.P. McNeal, N. Moelders, L. Last, W. Ho, A.C. Greenwald, J.T. Daly, I. Puscasu, E.A. Johnson, I. El-Kady and R. Biswas, Instrumentation for Air Pollution and Global Atmospheric Monitoring, 4574, 193 (2002).
8. B.J. Lee, Y.B. Chen and Z.M. Zhang, Opt Lett, 33, 204 (2008).
9. K. Joulain and A. Loizeau, Journal of Quantitative Spectroscopy & Radiative Transfer, 104, 208 (2007).
10. E.D. Palik, ed. *Handbook of Optical Constants of Solids*. Handbook of Optical Constants of Solids, ed. E.D. Palik. Vol. 1. 1998, Academic Press: San Diego.
11. W.L. Barnes, J Opt a-Pure Appl Op, 8, S87 (2006).
12. A.R. Ellis, H.M. Graham, M.B. Sinclair and J.C. Verley, Proceedings of the SPIE - The International Society for Optical Engineering, 706508 (9 pp.) (2008).